IEEE TRANSACTIONS ON

MAGNETICS

A PUBLICATION OF THE IEEE MAGNETICS SOCIETY

MARCH 1997 VOLUME 33 NUMBER 2 IEMGAQ (ISSN 0018-9464)

PART II OF TWO PARTS

SELECTED PAPERS FROM THE SEVENTH BIENNIAL IEEE CONFERENCE ON ELECTROMAGNETIC FIELD COMPUTATION (IEEE CEFC '96)

Okayama, Japan, March 18–20, 1996

(See p. 1125, Part II, for Conference on Electromagnetic Field Computation (IEEE CEFC '96) Table of Contents. CEFC papers begin on p. 1143. Regular papers begin on p. 1007, Part I.)

Finite Element Analysis of Steady State Behavior of Squirrel Cage Induction Motors Compared with Measurements.

R. De Weerdt and E. Tuinman
Holec Machines & Apparaten, Ringdijk 390, 2980 GB Ridderkerk, The Netherlands

K. Hameyer and R. Belmans
Katholieke Universiteit Leuven, Dept. EE, ESAT/ELEN, Kard. Mercierlaan 94, 3001 Leuven, Belgium

Abstract —**The paper describes the steady state analysis of squirrel cage induction motors using a two-dimensional finite element solution. Saturation is included using an iterative process combining both static and time-harmonic solutions. The motor end-effects are calculated using 2d and 3d finite elements including a lumped parameter approach during the solution of the time-harmonic problem. Both motors types, with closed and open rotor slots are analysed. Different operating points for load, no-load and locked rotor situations are analysed and compared. The influence of the different end-effect parameters is analysed by including or neglecting them in the calculations. Good agreement with measurements are found for all operating conditions. The calculations are performed using a commercial FEA package.**

I. Introduction

In the last decade, the analysis of squirrel cage induction motors using finite elements has received much attention. The analysis is mainly based on the field calculation of a cross-section of part of the motor (mostly one pole pitch). To obtain realistic results, the calculation must include the following effects:

1) Induced rotor currents
2) Saturation
3) Motor end effects

To combine both saturation and induced currents theoretically, a transient solution is required. Because this method results in very high computational costs, several approximation methods are developed [1,2]. The method described here uses a combination of static (non linear) and time-harmonic (linear) calculations. The motor end-effects (stator end-winding impedance and end-ring impedance) are included in the calculations as lumped parameters. Values for the end effect parameters are often obtained using empirical formulae. Here, the parameters are obtained by two- and three dimensional field analysis [3].

Manuscript received March 19,1996.
R. De Weerdt, tel. +31 1804 45624, fax +31 1804 45507; E. Tuinman, fax +31 1804 45507; R. Belmans, tel. +32 16 32 1020, fax +32 16 32 1985; K. Hameyer, Kay.Hameyer@ESAT.KULEUVEN.AC.BE, fax +32 16 32 1985.
The authors are indebted to the Belgian "NFWO", to the Belgian Ministry of Scientific Research for granting the project IUAP No. 51 on Magnetic Field and to Holec Machines & Apparaten, Ridderkerk, the Netherlands.

This results in a more accurate description of the end-effects. While the empirical formulae only give a single value for e.g. the end-winding leakage, the finite element analysis shows that the end-effect parameters vary under different load conditions. An additional advantage of calculating the end-effects is that no prototyping is required, the analysis is purely based on simulations.

II. Finite Element Analysis

Four-pole traction motors having 48 stator slots and 40 rotor slots are modeled. The 2d finite element model describes one pole pitch of the motor.

A. Combination of saturation and induced currents

To combine both the influence of induced currents and saturation, an iterative process using both time-harmonic and static solutions is used [2]. The time-harmonic solver is used to obtain the rotor currents. From the solution the real and imaginary part of stator and rotor currents are extracted and used as excitation for two static non linear problems. From the two static solutions, the reluctivity in each element is determined by averaging the reluctivities from the two solutions. The obtained reluctivity vector is used for the following time-harmonic (linear) solution. The described iteration procedure is found to converge in less than five steps and is more robust when compared to the method of successive underrelaxation [4]. It is used for both current driven and voltage driven calculations under various load conditions. The procedure can either be started with the static calculations (initially no rotor currents are assumed) or with the time-harmonic calculation. The latter is advantageous simulating open rotor slots. When closed rotor slots are examined, a linear calculation will provide much smaller rotor currents than the rated currents and will not influence the next static solution. Therefore, the iteration process should start with the static problem definition. The procedure gives similar results as the more conventional method of effective reluctivities [1]. The analysis is performed for motors with closed and open rotor slots.

B. Consideration of end-effects

The time-harmonic solution procedure consists of the finite element problem definition combined with a set of circuit

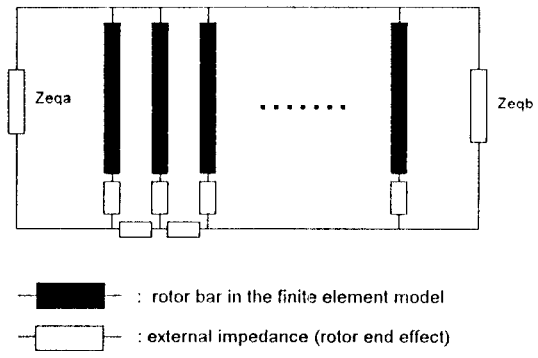

Fig. 1. Finite element - circuit model for one pole of a squirrel cage induction motor.

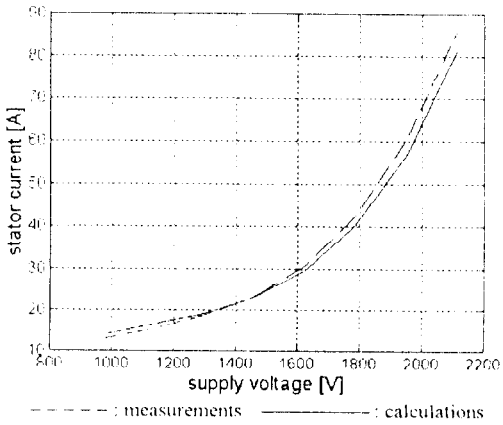

Fig. 2. Calculated and measured no-load characteristic.

equations describing the motor end-effects. The considered end-effects are the resistance and leakage inductance of both end-winding and end-ring. The end-effects are included as a lumped parameter model. The quantities of the parameters are obtained using the 2d and 3d finite element method as described in [3]. The end-winding parameters can be considered directly. The modeling of the end ring however, requires the inclusion of additional impedances. The 2d finite element model describes only one pole pitch of the motor geometry. Modeling only the part of the end-ring that exists between the rotor bars in the model would result in a time-harmonic solution with the sum of all bar currents to be zero. In order to obtain the correct solution the rotor model is expanded with two additional impedances Z_{eqa} and Z_{eqb} (Fig. 1).

In series with each rotor bar there is a resistance taking into account that the rotor bars are longer than the length of the iron core. Between two adjacent rotor bars an impedance equal to twice the ring segment impedance is placed. The enclosing impedances Z_{eqa} and Z_{eqb} are a function of the ring segment impedance Z_r, the number of pole-pairs p and the number of rotor bars N:

$$Z_{eqa} = Z_r + jZ_r cot\left(\frac{p\pi}{N}\right) \quad (1)$$

$$Z_{eqb} = Z_r - jZ_r cot\left(\frac{p\pi}{N}\right) \quad (2)$$

The influence of each separate end-effect parameter is examined by considering or respectively neglecting it in the simulation.

C. Calculation of the end-effect parameters

The calculation of the end effect parameters is performed using 2d and 3d finite elements except for the end-winding resistance, which is calculated analytically. The end-winding leakage and the end-ring leakage are calculated using a 3d model describing one pole pitch of the end-winding region. Both leakage components are calculated for different load conditions. An important variation in both parameters is noticed due to the fact that the coupling between stator end-winding and rotor end-ring is load-dependent [3]. This coupling between the end-winding and the end-ring should theoretically be incorporated in the magnetizing inductance but is negligible since the coupling mainly takes place in air. By far the most important end-effect parameter for a squirrel cage induction motor is the end-ring resistance. This parameter is calculated using an analytical approximation, a 2d (axisymmetric) and a 3d finite element calculation , also for different load conditions. Significant differences are obtained [3] when skin effect becomes important (motor start-up). Because the 3d approach is the only one where the current input is correctly modeled (via the bars), the 3d solution is considered the most accurate.

III. No-Load Simulation

For the no-load simulation, synchronous speed of the motor is assumed. Therefore, no induced rotor currents are assumed, the only end-effects that have to be taken into account are the end-winding impedances. The full end-winding inductance acts in this situation as leakage. Fig. 2 shows the calculated and measured no-load characteristic. It can be seen that the non linear behavior of the motor at no-load is correctly modeled.

The motor has closed rotor slots. The end-winding parameters have little influence on the overall result (less than 5%) because the end-winding leakage is only a few percent of the magnetizing inductance. The agreement with measurements is within 5% for most operating points both for motors with open and closed rotor slots.

IV. Load Simulation

For the load calculations, different operating points, at various values for the slip s, are compared with

measurements. As mentioned above, the time harmonic solver is used to obtain the induced rotor currents. For the no-load calculations it is merely used to obtain the stator currents when only the stator voltage is known (voltage driven no-load calculations). The time-harmonic solver however, requires that only one frequency is specified. During load operations, the frequency of the stator currents equals the supply frequency, while the rotor current frequency is the supply frequency multiplied by the slip. Two approaches are possible to resolve this problem.

Consider first the equation solved by the 2d time-harmonic solver (3).

$$\nabla\cdot(\nu\nabla A_z) - j\omega\sigma A_z = -J_{s,z} \tag{3}$$

Here A_z is z-component of the vector potential A, σ is the conductivity, ω is the angular velocity, $J_{s,z}$ is the source current and ν the reluctivity. To obtain the correct induced currents, the slip dependent angular velocity $s\omega_n$ (ω_n is the supplied angular velocity) can be applied in (3) resulting in the following equation to be solved (4):

$$\nabla\cdot(\nu\nabla A_z) - js\omega_n\sigma A_z = -J_{s,z} \tag{4}$$

For voltage driven calculations, applying the slip pulsation is not sufficient. When the slip pulsation is used, the flux variation on the stator will also take place with this pulsation resulting in a back-EMF that is 1/s times smaller than required. Therefore, the applied voltage U_n has to be scaled down to sU_n. In order to maintain the correct ratio between back-EMF and resistive voltage drop, the resistivity of the stator winding has to be scaled down in the same manner.

Equation (4) suggest an other possibility: It is possible to obtain the correct induced currents by applying the supply frequency and simultaneously using $s\sigma$ as the conductivity in the rotor. This approach is used here since it requires the modification of the rotor conductivity only, the supply voltage and stator resistance keep their rated value. It should be noted that the modified conductivity should also be used to calculate the rotor end ring resistance and the resistance of the bar ends outside the rotor core (Fig. 1).

A. Comparison between measurements and simulations

Table I shows a comparison of calculated and measured quantities for the stator current I, the supply power P and the torque T at different values for the slip s.

TABLE I
COMPARISON BETWEEN CALCULATED AND MEASURED LOAD OPERATING POINTS

slip s [%]	I [A] (a) CALCULATIONS	I [A] (b) MEASUREMENTS	P [kW] (a)	P [kW] (b)	T [Nm] (a)	T [Nm] (b)
2.01	91.7	89.0	245	234	1321	1257
1.68	78.9	75.6	208	196	1126	1060
1.21	59.9	59.3	153	148	835	801
0.80	43.9	45.2	103	103	562	552
0.34	27.5	30.5	42	46	242	234

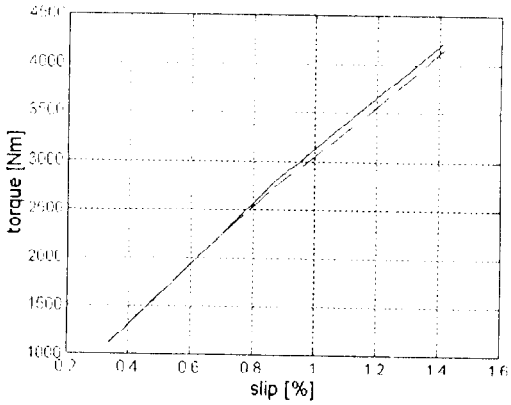

Fig. 3. Measured and calculated torque characteristic for a 400 kW traction motor.

Good agreement between calculation and measurement can be taken from table I. The comparison shown in table I is done for a motor with closed rotor slots and a rated power of 146 kW. The main reason why the calculated power and current are smaller than measured is that iron losses are not incorporated in the calculations.

Fig. 3 shows the torque characteristic (measurements and calculations) for a 400 kW motor with open slots.

B. Influence of the end-effect parameters

All four end-effect parameters mentioned above have to be taken into account. The most important end-effect parameter is the end-ring resistance. Calculations show that more than 30 % of the Joule losses in the rotor are located in the bar-ends outside the rotor core and in the end-ring. The generated torque of the motor is proportional to the rotor Joule losses. Therefore, an accurate calculation and consideration of the end-ring resistance is essential. Furthermore, due to the small slip frequency, it can be stated that the end-ring leakage is of no importance during load operations. As it is in the no-load simulations, the influence of the end-winding impedance remains small. This is enforced by the fact that the end-winding leakage is smaller during load operations.

V. LOCKED ROTOR SIMULATIONS

For motors with open rotor slots, the behavior at locked rotor operation is approximately linear. The above described procedure converges in two iteration steps. For motors with closed rotor slots, the consideration of saturation cannot be neglected, the behavior is non linear. Also the influence of the different end-effect parameters is different for both types of motors.

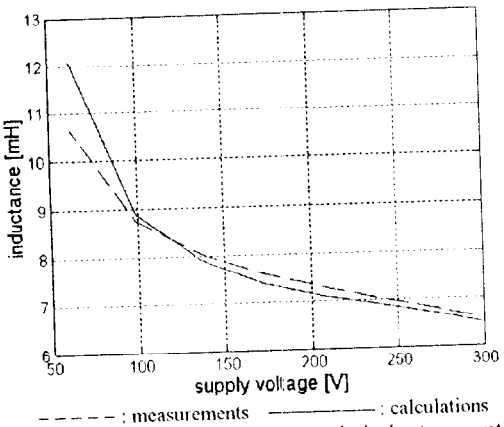

Fig. 4. Measured and calculated inductance at locked rotor operation (closed rotor slots).

A. Comparison between measurements and simulations

Fig. 4 shows the calculated and measured locked rotor inductance for various values of the supply voltage.

Good agreement with measurements is found for most operating points. The non linear behavior of the motors with closed rotor slots is mainly due to an additional leakage component, the bridge leakage, that is strongly load dependent [5].

B. Influence of the end-effect parameters

During locked rotor operation, none of the end-effect parameters can be neglected even though the leakage components of end-winding and end-ring are at their minimum value. During locked rotor operation the coupling between rotor end-ring and stator end-winding obtains its maximum value, so the leakage parts of end-winding inductance and end-ring inductances are at their minimum value [3].

Table II shows a comparison of calculated and measured values for the stator current I, the supply power P, inductance L and resistance R for locked rotor operation. The influence of the different end-effect parameters is shown by including them one by one in the simulation. Table II refers to a motor with open rotor slots.Only if all end-effect parameters are considered, good agreement with measurements are found. Unlike in the load or no-load calculation, the end-ring leakage has a distinct influence at locked rotor operation. This holds only for motors with open slots. Due to the bridge leakage the influence of the end-ring leakage is much smaller for motors with closed rotor slots.

TABLE II
COMPARISON BETWEEN CALCULATED AND MEASURED LOCKED ROTOR OPERATION (a) CALCULATIONS, (b) MEASUREMENT

	I[A]	P [kW]	L [mH]	R [mΩ]
(a1)	197.4	16.1	2.6	138
(a2)	160.4	14.1	2.6	183
(a3)	159.4	14.0	3.1	184
(a4)	158.7	15.6	3.1	207
(a5)	152.9	14.2	3.2	207
(b)	152.0	14.3	3.2	208

The different simulations of table II are:
(a1) : no end effects included
(a2) : inclusion of end winding resistance
(a3) : inclusion of end winding impedance
(a4) : (a3) plus inclusion of end ring resistance
(a5) : inclusion of all end effect parameters

VI. CONCLUSIONS

The analysis of squirrel cage induction motors is performed and compared with measurements. The end-effect parameters are included as lumped parameters in the 2d analysis. The influence of the end-effect parameters is examined for all load conditions by including or neglecting them in the calculations. Good agreement between measurements and computations is found.

At no-load, the influence of the end-winding impedance is noticeable but rather small (less than 5%).

At load, the most important parameter is the end-ring resistance. The end-winding leakage inductance has little influence and the end-ring leakage inductance can be neglected.

For motors with open rotor slots examined at locked rotor, all end-effect parameters have a significant influence on the motor behavior. For motors with closed rotor slots, the end-ring leakage has far less influence. This is due to the fact that these motors have an additional leakage component, the bridge leakage, that also results in a non linear behavior at locked rotor operation.

REFERENCES

[1] E. Vassent, G. Meunier and J.C. Sabonnadière, "Simulation of induction machine operation using complex magnetodynamic finite elements," *IEEE Trans. on Magnetics*, Vol. 25, No. 4, 1989, pp. 3064-3066.

[2] R. Belmans, R. De Weerdt and E. Tuinman, "Combined field analysis techniques and macroscopic parameter simulation for describing the behaviour of medium-sized squirrel-cage induction motors fed with an arbitrary voltage," EPE Brighton, September 1993, pp. 413-418.

[3] R. De Weerdt and R. Belmans, "Squirrel cage induction motor end effects using 2D and 3D finite elements," EMD Durham, September 1995, pp 62-66.

[4] R. De Weerdt, K. Brandiski, U. Pahner and R. Belmans, "Comparative analysis of two methods for time-harmonic solution of the steady state in induction motors," *J. Appl. Phys.* 75 (10), Proc. of the 38th Annual Conference on Magnetism and Magnetic Materials, p. 6050.

[5] S. Williamson and M.C. Begg, "Calculation of the bar resistance and leakage reactance of cage rotors with closed slots", *IEE Proc.* Vol. 132, Pt. B, No. 3, 1985, pp. 125-132.